Journal of Medicinal Chemistry

Article

pubs.acs.org/jmc

Discovery, Synthesis, and Biological Evaluation of Orally Active Pyrrolidone Derivatives as Novel Inhibitors of p53−MDM2 Protein−Protein Interaction

Chunlin Zhuang,[†] Zhenyuan Miao,[†] Lingjian Zhu, Guoqiang Dong, Zizhao Guo, Shengzheng Wang, Yongqiang Zhang, Yuelin Wu, Jianzhong Yao, Chunquan Sheng,* and Wannian Zhang*

School of Pharmacy, Second Military Medical University, 325 Guohe Road, Shanghai 200433, People's Republic of China

Supporting Information

ABSTRACT: The p53−MDM2 interaction has been proved to be a valuable target to develop effective antitumor agents. Novel p53−MDM2 inhibitors bearing pyrrolidone scaffolds were successfully identified by structure-based design. The nanomolar inhibitor **5** possessed good p53−MDM2 inhibitory activity (K_i = 780 nM) due to its hydrophobic and hydrogen bonding interactions with MDM2. Further hit optimization led to the discovery of a number of highly potent pyrrolidone derivatives with improved p53−MDM2 inhibitory activity and in vitro antiproliferative potency. Compounds **41** (K_i = 260.0 nM) and **60a** (K_i = 150.0 nM) showed good and selective activity against tumor cells with deleted p53. In addition, these two compounds also effectively inhibited the tumor growth in the A549 xenograft model. Interestingly, compound **41** was proved to be a potent MDM2/MDMX dual inhibitor. The novel pyrrolidone p53−MDM2 inhibitors represent promising lead structures for the development of novel antitumor agents.

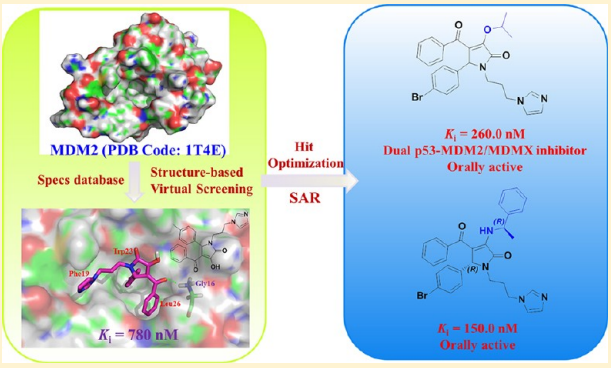

INTRODUCTION

The p53 tumor suppressor is a potent transcription factor that plays a crucial role in DNA repair, differentiation, senescence, apoptosis, and cell-cycle arrest.[1,2] It is also the most frequently inactivated protein in human cancer. In more than 50% of all human cancers, the p53 gene is deleted or mutated.[3,4] For the remaining half of the cancers, the p53 that retains its wild-type form is tightly controlled by the human murine double minute 2 (MDM2) oncoprotein through an autoregulatory feedback loop.[5−9] Inhibitors of the p53−MDM2 binding interaction are expected to restore normal p53 activity in MDM2-over-expressing cells and thus exert antitumor effects.[3]

However, the inhibition of protein−protein interactions is a challenging task for drug discovery because most protein−protein interactions occur over large surface areas with relatively flat topologies and nondescript surfaces.[6−10] For the p53−MDM2 interface, it is a narrow and deep cleft which is different from many other protein−protein interfaces.[11] The α-helix of p53 (residues 15−29) is inserted into the groove of MDM2 and primarily makes hydrophobic contacts with MDM2. There are three relatively small binding pockets (i.e., Phe19 pocket, Trp23 pocket, Leu26 pocket) on MDM2 for p53 binding, which are suitable for the design of small-molecule inhibitors.[12] Because of the importance of p53−MDM2 as a therapeutic target, several nonpeptide inhibitors have been reported in recent years.[13] These small-molecule inhibitors mainly include chalcones,[14,15] piperazine-4-phenyl derivatives,[16] chlorofusins,[17] norbornanes,[10] nutlins,[18] sulfonamides,[19] benzodiazepinediones,[20] isoindolinones,[19] terphenyls,[21] spiro-oxindoles,[22] and quinolinols.[23] However, the majority of them showed weak inhibitory activity of the p53−MDM2 interaction. Among them, the most potent p53−MDM2 inhibitors are the nutlins (e.g., nutlin-3a, Figure 1), benzodiazepines (e.g., TDP222669, Figure 1), and spiro-oxindoles (e.g., MI-219, Figure 1).

The nutlins were identified by high throughput screening at Roche.[18] Further optimization led to a promising candidate with potent in vitro and in vivo activities.[18] The X-ray crystal structures revealed that nutlins bound to the p53 binding site of MDM2 by mimicking the p53 peptide to a high degree.[18] Recently, Roche reported on its web site that one of its inhibitors (RG7112) has entered phase I clinical trials.[13] Spiro-oxindoles were discovered by structure-based de novo design[22] and represented another class of promising inhibitors that are in clinical development. Initially, Wang's group discovered MI-219 as a potent, specific, cell-permeable, and orally active small-molecule inhibitor. Further optimization of MI-219 led to a more potent analogue (MI-319).[24] This compound also exhibited potent activities against follicular lymphoma that retains wild-type p53 both in vitro and in vivo. In addition, MI-319 in combination with cisplatin induced cell growth

Received: June 24, 2012
Published: October 9, 2012

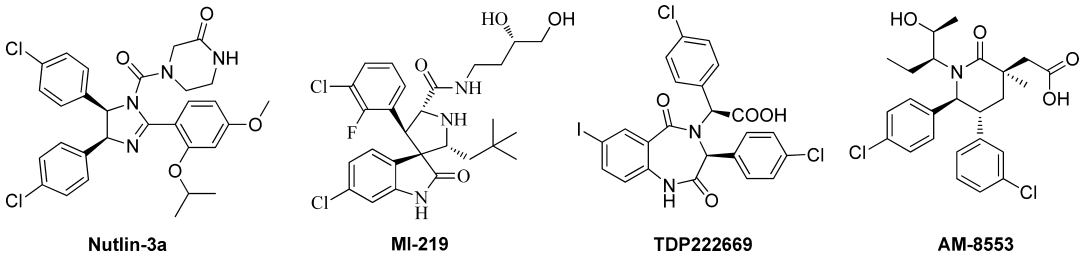

Figure 1. Representative small molecule p53−MDM2 inhibitors.

Scheme 1. [a]

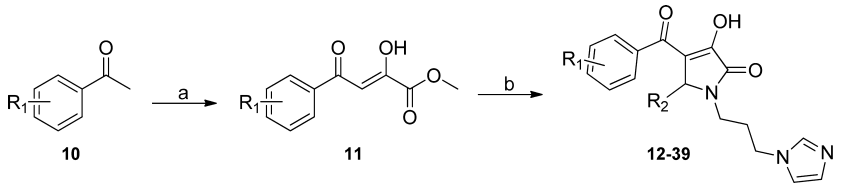

[a]Reagents and conditions: (a) ethyl oxalate, CH_3ONa/CH_3OH, reflux, 3 h; (b) R_2CHO, *N*-(3-aminopropyl)imidazole, 1,4-dioxane, room temperature, 12 h, yield: 14.2−80.1%.

inhibition and apoptosis in pancreatic cancer cells irrespective of their p53 mutational status.[25] Encouragingly, a clinical candidate derived from MI-319 has entered phase I clinical trials. Very recently, a novel class of a piperidinone scaffold has been designed using a structure-based de novo design strategy. Among the optimized MDM2 inhibitors, AM-8553 (Figure 1) has a promising outlook for potential clinical development.[26,27]

The structures of the nutlins, spiro-oxindoles, and benzodiazepines seem quite different, but they all share common structural features: (1) two *cis*-phenyl groups to ensure the hydrophobic interactions, and (2) the functional groups that are capable of forming hydrogen-bonding interactions. Meanwhile, cocrystal structures and docking studies indicated that their binding mode mimicked that of p53 peptide.[28] So far, small-molecule inhibitors of MDM2 are all designed to mimic the residues Phe19, Trp23, and Leu26 in p53 and their interactions with MDM2.[20] Although the potential benefits for the inhibition of the p53−MDM2 protein−protein interaction have been recognized for nearly 20 years, there are currently still limited classes of highly potent small-molecule inhibitors that show potent antitumor efficacy.[29] Thus, it is highly desirable to discover novel chemotypes that possess high p53−MDM2 inhibitory activities and suitable drug-like properties. Continuing our efforts in designing novel inhibitors of the p53−MDM2 interaction,[30] we herein report the discovery and optimization of novel pyrrolidone inhibitors that showed both nanomolar inhibitory activities toward p53−MDM2 interaction and potent in vivo antitumor efficacy. Interestingly, several highly active pyrrolidone derivatives were found to act by dual inhibition of p53−MDM2 and p53−MDMX interactions.

CHEMISTRY

As depicted in Scheme 1, the pyrrolidone derivatives were synthesized via a simple two-step procedure. In the first step, substituted methyl pyruvates **11** were obtained by Claisen condensation of aryl methyl ketones **10** with ethyl oxalate.[31,32] Then, pyruvates **11** were reacted with *N*-(3-aminopropyl)-imidazole and aldehydes to afford authentic compounds **12−39** by a highly efficient three-component coupling reaction.[33] In the lead optimization stage, the ether-pyrrolidone derivatives **40−47** were synthesized by Mitsunobu reaction between compound **32** and various alcohols (Scheme 2). The amino-substituted pyrrolidone derivatives **48−60** were obtained by Leuckart−Wallach reaction under microwave conditions (Schemes 3 and 4).

Scheme 2. [a]

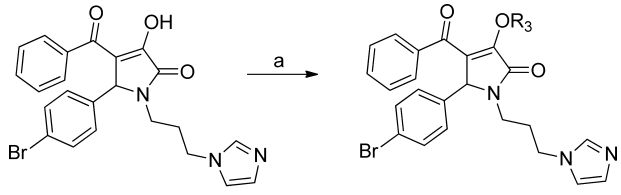

[a]Reagents and conditions: (a) PPh_3, DIAD, THF, R_3OH, room temperature, 12 h, yield: 21.3−67.6%.

RESULTS AND DISCUSSION

Virtual Screening and p53−MDM2 Binding Assay. Virtual screening offers a practical strategy to identify new leads for drug discovery.[34] Previously, Wang's group successfully discovered quinolinol inhibitors of p53−MDM2 interaction by computational screening of the NCI 3D database.[23] Encouraged by the results, we performed a structure-based virtual screening study to search a new molecular database, namely the Specs database,[35] to find novel types of p53−MDM2 inhibitors (see Supporting Information for details of virtual screening). The binding K_i constants of the 25 selected candidate compounds were measured by the fluorescence polarization (FP) binding assay.[22,23,36] Nutlin-3a, one of the most active small-molecule p53−MDM2 inhibitors, was used as the reference drug.[18] To our delight, nine hits were identified to possess p53−MDM2 inhibitory activity with K_i values ranging from 0.57 μM to 85.97 μM (Figure 2; the binding curves can be found in the Supporting Information). Interestingly, the pyrrolidone framework turned out to be a privileged scaffold among the identified hits. Six out of nine hits, including two

dx.doi.org/10.1021/jm300969t | J. Med. Chem. 2012, 55, 9630−9642

Scheme 3. [a]

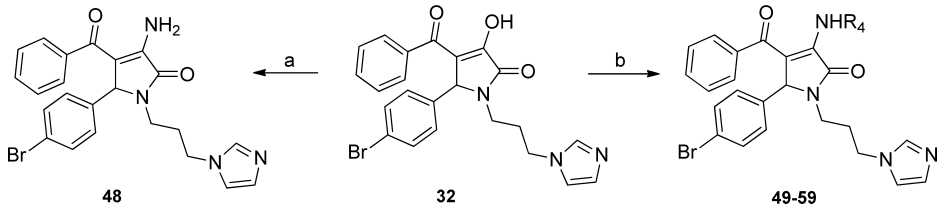

[a]Reagents and conditions: (a) NH_4COOH, 2-methoxyethanol, microwave, 150 °C, 1 h, yield: 32.0%; (b) R_4NH_2, CH_3COOH, microwave, 120 °C, 2 h, yield: 17.9−55.9%.

Scheme 4. [a]

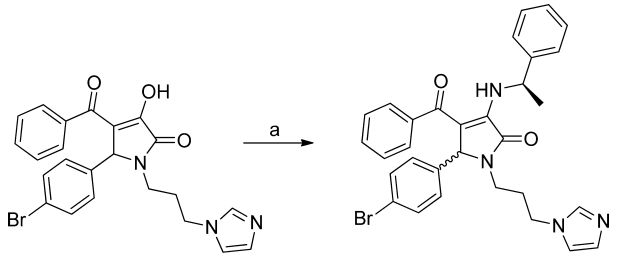

[a]Reagents and conditions: (a) *R*-α-phenylethylamine, CH_3COOH, microwave, 120 °C, 2 h, yield: 6.93%, 10.3%.

nanomolar inhibitors (**5** and **9**), have a common pyrrolidone scaffold, which was completely different from the reported p53−MDM2 inhibitors. Moreover, the pyrrolidone analogues were recently designed as inhibitors of the Annexin A2-S100A10 protein−protein interaction,[37] highlighting the importance of the pyrrolidone scaffold for the design of small-molecule inhibitors of protein−protein interactions. Among the identified hits, compounds **5** and **9** displayed excellent p53−MDM2 inhibitory activity, with K_i values of 780 nM and 570 nM, respectively, which were comparable to that of the positive drug nutlin-3a.

To obtain the accurate binding mode of these hits, molecular dynamics (MD) simulations were performed on the docking model of compounds **1**, **5**, **6**, and **9**. As shown in Figure 3, the binding of these compounds with MDM2 is primarily mediated

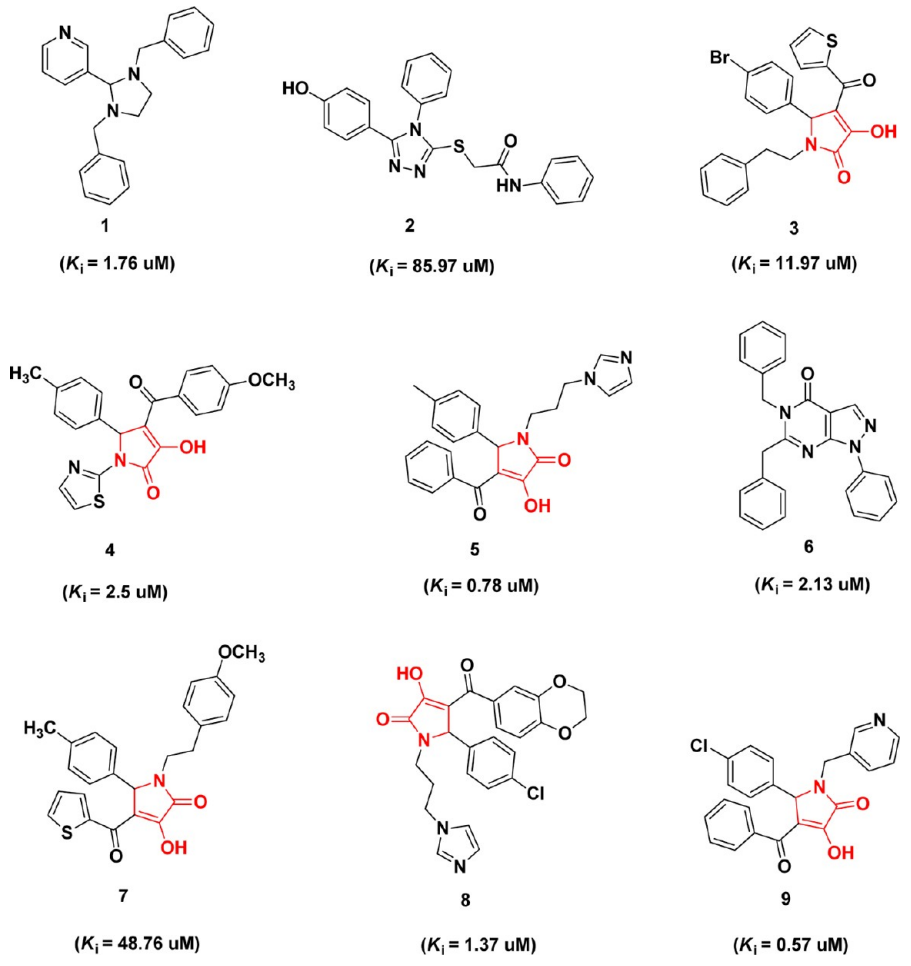

Figure 2. Chemical structures and p53−MDM2 inhibitory activities of hits from structure-based virtual screening.

dx.doi.org/10.1021/jm300969t | J. Med. Chem. 2012, 55, 9630−9642

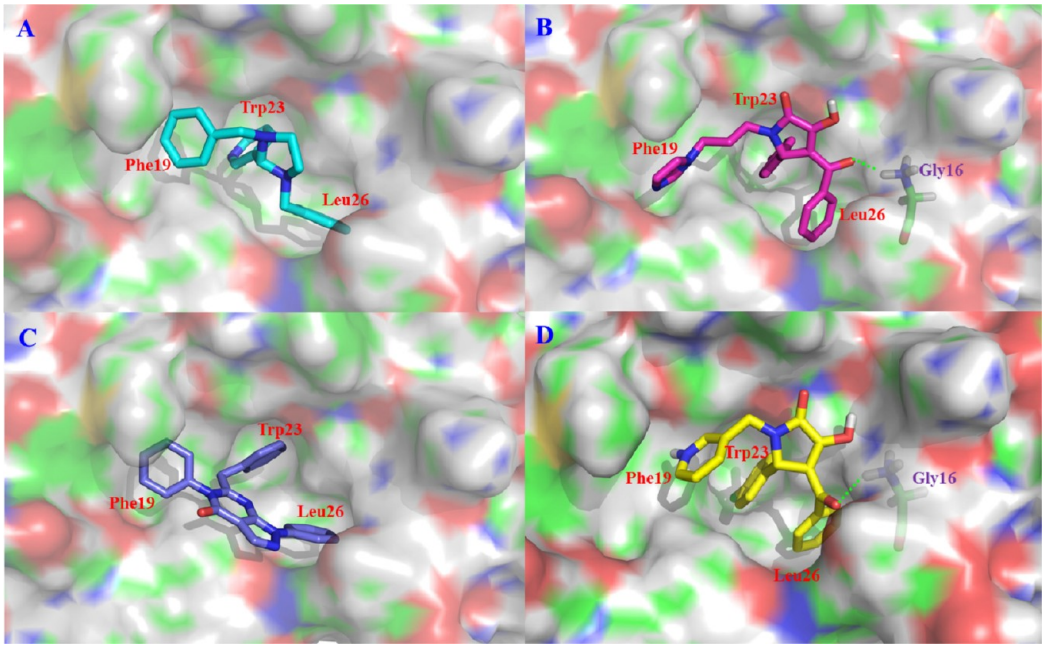

Figure 3. Binding modes of four hits in three key subpockets of MDM2: (A) Compound **1**, (B) compound **5**, (C) compound **6**, (D) compound **9**. The figure was generated using PyMol (http://pymol.sourceforge.net/).

by extensive hydrophobic interactions. Three aromatic substituents of the scaffolds mimic the three key residues (Phe19, Trp23, and Leu26) of p53. For example, compounds **5** and **9** interact with MDM2 by filling its Trp23 subpocket with their 5-substituted group. The N-substituted and 4-substituted groups are located in the Phe19 and Leu26 pockets, respectively. Compounds **1** and **6** did not form direct hydrogen bonds with MDM2. In contrast, the pyrrolidone derivatives **5** and **9** can form additional hydrogen bonding interaction with the backbone of Gly16. As a result, these two compounds showed relatively higher inhibitory activity.

Hit Optimization and Structure–Activity Relationships. The pyrrolidone p53–MDM2 inhibitors represent a novel chemotype for the development of highly potent p53–MDM2 inhibitors. Because the solubility of compound **5** was better than that of compound **9**, compound **5** was chosen for further structural optimization. The optimization studies were focused on improving the affinity with MDM2 as well as the physicochemical properties. First, various substitutions were introduced on the C5-phenyl of the pyrrolidone derivative **5** (compounds **12**–**32**). The fluorescence polarization assay revealed that seven compounds in this series (**12**, **20**, **23**, **26**, **27**, **29**, **32**) possessed potent activity with IC_{50} values lower than 1 μM (Table 1). Particularly, the 4-bromo derivative **32** (K_i = 0.29 μM) showed high binding affinity comparable to the positive drug nutlin-3a (K_i = 0.23 μM). Structure–activity relationship (SAR) analysis demonstrated that the type and position of the substitutions were important for the inhibitory activity. The replacement of the methyl of group of hit **5** by a bromine (compound **32**) or nitro group (compound **29**, K_i = 0.70 μM) led to the increased activity. The 4-fluoro derivative **12** (K_i = 0.88 μM) and the 4-trifluoromethyl derivative **26** (K_i = 0.81 μM) also showed activity comparable to that of compound **5**. However, decreased inhibitory activity was observed for the 4-chloro derivative **14** (K_i = 23.35 μM) and 4-*tert*-butyl derivative **25** (K_i = 10.90 μM), and the 4-methoxyl derivative **16** was totally inactive. When the bromine atom of compound **5** was moved to position 2 (compound **27**), excellent inhibitory activity was also observed (K_i = 0.43 μM). Similarly, movement of the 4-nitro group of compound **29** to position 3 generated compound **21** (K_i = 0.83 μM), with comparable activity. Because the phenyl group of compound **5** was located in the hydrophobic Phe19 pocket, the introduction of a hydrophilic hydroxyl group on the phenyl ring (compounds **19** and **20**) resulted in the loss of the activity. Two 2,4-disubstituted compounds, **13** and **21**, only showed moderate activity. In contrast, good inhibitory activity was retained for 3,5-dimethyl derivative **23** (K_i = 0.91 μM). When the phenyl group of compound **5** was replaced by various heterocycles or other aromatic groups, such as pyridine (**15**, **22**, **24**), thiophene (**17**, **28**), furan (**31**), and naphthalene (**18**), the loss of p53–MDM2 inhibitory activity was observed for them. The results highlighted the importance of the phenyl group of compound **5** for the binding with MDM2.

Because the 4-bromo group was found to be the most favorable substitution for the C5-phenyl group, compound **32** was further optimized by introducing various substitutions on its C4-benzoyl group. Unfortunately, compounds **33**–**39** showed decreased activity. The 4-chloro derivative **37** was more active than the 4-fluoro (**38**), 4-nitro (**34**), 4-iodo (**39**), and 4-bromo (**33**) derivatives, but it was less potent than the unsubstituted compound **32**. Next, optimization studies were focused on introducing substituents on the C3-hydroxyl group of the pyrrole ring. A series of ether-pyrrolidone derivatives (compounds **40**–**47**) were designed and synthesized. The in vitro assay revealed that most of them showed nanomolar binding activity to MDM2 (Table 2). Particularly, the p53–MDM2 inhibitory activity of compound **41** was comparable to that of the positive drug nutlin-3a. SAR analysis indicated that the aliphatic substituents, except for the propyl group, were more favorable than the benzyl group.

Encouraged by the results, we further replaced the hydroxyl group of compound **32** by the amine group to generate compound **48**. Interestingly, the inhibitory activity of

dx.doi.org/10.1021/jm300969t | *J. Med. Chem.* 2012, 55, 9630–9642

Table 1. MDM2 Binding Affinity of Compounds 12−39

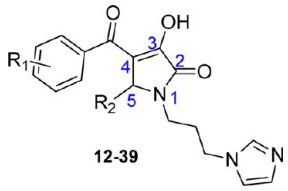

12-39

compound	R_1	R_2	K_i[a] (μM)
12	H	4-F-Ph	0.88
13	H	2,4-di-CH_3-Ph	10.7
14	H	4-Cl-Ph	23.35
15	H	6-Cl-pyridin-3-yl	n.a.
16	H	4-OCH_3-Ph	n.a.
17	H	thiophen-3-yl	n.a.
18	H	naphthalen-2-yl	n.a.
19	H	3-OH-Ph	n.a.
20	H	3-NO_2-Ph	0.83
21	H	2,4-diCl-Ph	39.43
22	H	pyridin-2-yl	n.a.
23	H	3,5-di-CH_3-Ph	0.91
24	H	pyridin-3-yl	n.a.
25	H	4-$C(CH_3)_3$-Ph	10.90
26	H	4-CF_3-Ph	0.81
27	H	2-Br-Ph	0.43
28	H	thiophen-2-yl	n.a.
29	H	4-NO_2-Ph	0.70
30	H	2-OH-Ph	n.a.
31	H	furan-2-yl	n.a.
32	H	4-Br-Ph	0.29
33	4-Br	4-Br-Ph	24.87
34	4-NO_2	4-Br-Ph	2.54
35	2-NO_2	4-Br-Ph	15.29
36	2-Cl	4-Br-Ph	n.a.
37	4-Cl	4-Br-Ph	0.91
38	4-F	4-Br-Ph	1.46
39	4-I	4-Br-Ph	3.59
nutlin-3a	–	–	0.23

[a]Values were determined by fluorescence polarization assay. n.a. = not active.

Table 2. MDM2 Binding Affinity of Compounds 40−47

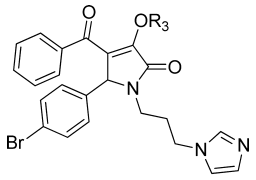

40-47

compound	R_3	K_i[a] (μM)
32	–	0.29
40	CH_2CH_3	0.69
41	$CH(CH_3)_2$	0.26
42	$(CH_2)_4CH_3$	0.34
43	$(CH_2)_3CH_3$	0.47
44	cyclohexyl	0.49
45	CH_2Ph	2.07
46	$CH_2CH_2OCH_3$	1.34
47	$CH_2CH_2CH_3$	6.97
nutlin-3a	–	0.23

[a]Values were determined by fluorescence polarization assay.

Table 3. MDM2 Binding Affinity of Compounds 48−60

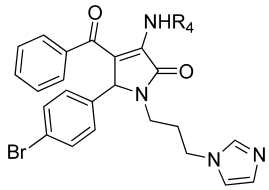

64-76

compound	R_4	K_i[a] (μM)
32	–	0.29
48	H	0.048
49	Ph	0.14
50	4-CH_3-Ph	0.14
51	4-OCH_2CH_3-Ph	0.35
52	4-F-Ph	0.43
53	4-I-Ph	0.27
54	4-Br-Ph	0.19
55	4-Cl-Ph	0.23
56	4-OCF_3-Ph	0.12
57	3-Br-Ph	0.15
58	2-Br-Ph	0.15
59	CH_2Ph	0.47
60a	(*R*)-1-phenylethyl	0.15
60b	(*R*)-1-phenylethyl	n.a.
nutlin-3a	–	0.23

[a]Values were determined by fluorescence polarization assay.

compound **48** was significantly improved (K_i = 48.0 nM, Table 3), whose activity was 5 times higher than that of compound **32**. The predicted binding mode indicated that the amino group formed an additional hydrogen bond with His96 (Figure 4A). When the amino group of compound **48** was substituted by various aromatic groups (compounds **49**−**59**), the p53−MDM2 inhibitory activity was slightly decreased. However, compounds **49**−**59** were also active in the nanomolar range (K_i range: 0.12 μM to 0.47 μM), and most of them were more potent than nutlin-3a. Moreover, they were more soluble than compound **48**. Interestingly, when compound **32** was treated with (*R*)-α-phenylethylamine, two diastereoisomers (**60a** and **60b**) could be obtained. In the p53−MDM2 binding assay, these two diastereoisomers showed different activity. Compound **60a** had a K_i value of 0.15 μM, whereas compound **60b** was totally inactive. The above results demonstrated that conformational restriction may be an important factor for improving biological activities of this class of compounds. To determine the absolute configuration of the diastereoisomers, electronic circular dichroism (ECD) was applied for configurational and conformational analysis. The overall predicted ECD spectrum of **60a** was subsequently compared with the experimental data, which revealed a good agreement between the calculated and measured ECD curves (see Supporting Information for details). Thus, the configuration of compound **60a** was established as (*R*,*R*). Further docking studies revealed that the amine group of compound **60a** formed a new hydrogen bond with Ser17 instead of His96 (Figure 4B).

In Vitro Antiproliferative Activity. To investigate the in vitro antiproliferative activity of the potent p53−MDM2 inhibitors, four human tumor cell lines, namely U-2 OS (wild-type p53), A549 (wild-type p53), Saos-2(p53 null), and NCI-H2119 (p53 null), were chosen for assaying. Nutlin-3a

dx.doi.org/10.1021/jm300969t | J. Med. Chem. 2012, 55, 9630−9642

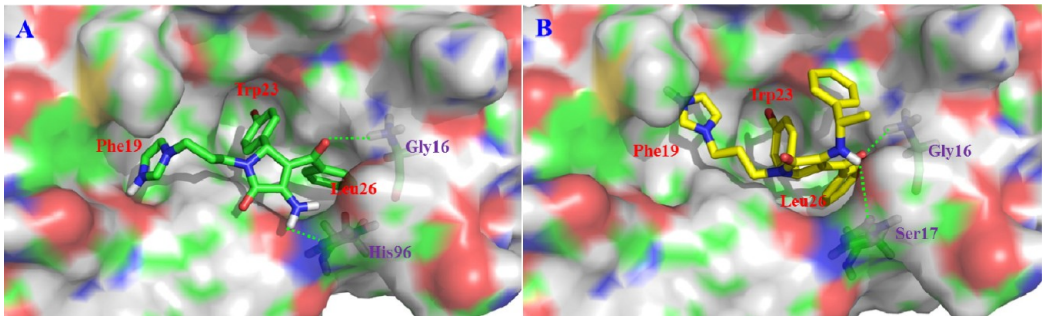

Figure 4. Schematic representation of the proposed binding mode for compound **48** (A) and compound **60a** (B). The figure was generated using PyMol (http://pymol.sourceforge.net/).

was used as a reference agent. The obtained IC_{50} values for the optimized nanomolar p53−MDM2 inhibitors are summarized in Table 4. In general, these p53−MDM2 inhibitors displayed moderate to good activity against cancer cell lines with wild-type p53. As compared with compound **32**, the ether-pyrrolidone derivatives showed improved antiproliferative activities. Particularly, compounds **41** (IC_{50} = 8.72 μM) and **42** (IC_{50} = 7.29 μM) showed better activity against the A549 cell line than nutlin-3a (IC_{50} = 15.12 μM). Compound **42** was also more active against the U-2 OS cell line (IC_{50} = 9.14 μM) than nutlin-3a (IC_{50} = 14.31 μM).

Table 4. In Vitro Antiproliferative Activities of the Selected Compounds

	IC_{50}[a] (μM)			
compound	Saos-2	U-2 OS	A549	NCI-H1299
32	31.62	n.a.	73.06	19.99
40	31.68	21.88	35.25	28.86
41	22.97	24.83	8.72	18.87
42	9.99	9.14	7.29	10.26
43	11.63	32.35	18.52	17.11
44	29.68	22.43	31.2	19.88
48	106.9	148.67	n.a.	168.5
49	24.38	25.67	24.14	21.18
50	31.87	24.12	29.38	25.76
51	30.85	26.17	20.21	19.95
52	32.69	30.01	27.35	25.44
53	23.38	12.01	24.52	19.35
54	23.75	12.99	22.23	19.25
55	24.76	22.8	29.95	25.04
56	17.87	11.51	20.82	11.48
57	9.09	11.86	15.77	11.54
58	19.62	16.91	20.07	15.62
59	31.6	32.48	52.77	25.28
60a	27.45	28.11	1.97	14.36
60b	13.17	30.83	15.70	17.00
nutlin-3a	31.62	14.31	15.12	20.48

[a]Values were measured with the MTT method. n.a. = not active.

However, the antitumor activity of compound **48**, the most active p53−MDM2 inhibitor, was weak mainly because of its poor solubility. Fortunately, its amine-substituted derivatives showed enhanced in vitro antiproliferative activities. Compounds **53**, **54**, **56**, and **57** revealed better inhibitory activities against the U-2 OS cell line with wild-type p53 than nutlin-3a. In particular, compound **60a** showed the best inhibitory effect (IC_{50} = 1.97 μM) against lung cancer A549 cell line (wild-type p53), which was much higher than that of nutlin-3a (IC_{50} = 15.12 μM). Furthermore, its IC_{50} value against the lung cancer NCI-H1299 cell line (p53 null) was 14.36 μM, demonstrating the selectivity of compound **60a** over cancer cell lines with deleted p53. Among the synthesized pyrrolidone derivatives, compounds **41** and **60a** showed both high p53−MDM2 inhibitory activities and potent in vitro antiproliferative activities with selectivity over cancer cell lines with deleted p53. Moreover, suitable solubility was also observed for them, and thus they were chosen for further mechanism and in vivo studies.

Western Blot Assay. The inhibition of the p53−MDM2 interaction is expected to activate p53, resulting in an increased level in the cells with wild-type p53.[38−40] In addition, activation of p53 can also lead to an increase in the levels of $p21^{cip1/waf}$ and MDM2 proteins.[18] To test these predictions, cells were lysed at 24 h and protein extracts were analyzed by Western immunoblotting for the levels of p53, MDM2, and $p21^{cip1/waf}$ proteins in A549 cancer cells that were treated with compound **60a** and nutlin-3a. Consistent with the predictions, compound **60a** caused a dose-dependent increase in the levels of p53, MDM2, and $p21^{cip1/waf}$ proteins in A549 cells (Figure 5), indicating a good activation of p53. Especially for MDM2, compound **60a** was more active than nutlin-3a.

MDMX Binding Assay. MDMX, a homologue of MDM2, has a distinct but complementary mode of action with MDM2

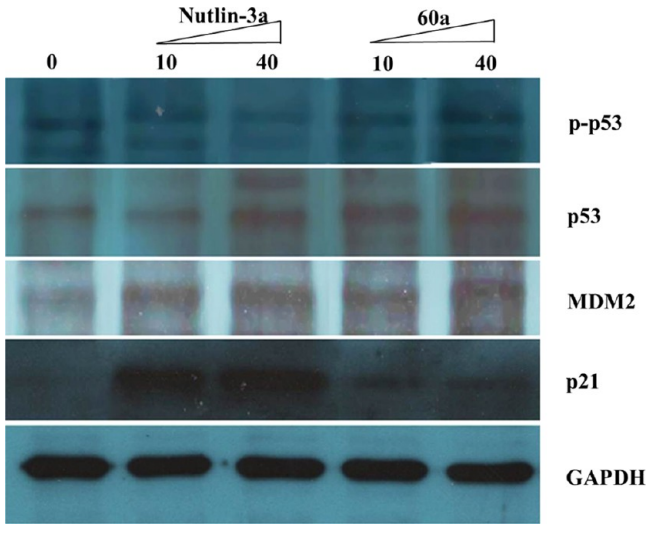

Figure 5. Cellular activity of nutlin-3a and **60a** for the p53 pathway activation detected by Western blotting (A549 cells, 24 h treatment).

dx.doi.org/10.1021/jm300969t | J. Med. Chem. 2012, 55, 9630−9642

in the regulation of the pro-apoptotic activity of p53.[41] Recent data indicated that the development of dual inhibitors of the two oncogenic proteins could result in more effective antitumor agents.[42−45] Although many MDM2 inhibitors have been reported, no potent small molecule inhibitor has been reported to tightly bind to MDMX despite the slight differences between MDM2 and MDMX pockets (RMSD for main chain atoms: 1.22 Å).[46−48] To investigate the MDMX inhibitory efforts of the pyrrolidone derivatives, compounds **41** and **60a** were subjected to MDMX binding assay (Table 5). Interestingly,

Table 5. MDMX Binding Affinity of the Selected Compounds

compound	K_i^a (μM)	compound	K_i^a (μM)
32	n.a.	**45**	n.a.
40	38.91	**46**	2.11
41	2.68	**47**	9.32
42	n.a.	**48**	n.a.
43	n.a.	**60a**	n.a.
44	17.93	nutlin-3a	5.86

[a]Values were determined by fluorescence polarization assay. n.a. = not active.

compound **57** showed good MDMX inhibitory activity (K_i = 2.68 μM), which was more potent than nutlin 3a (K_i = 5.86 μM). In comparison, compound **60a** was inactive against MDMX. Furthermore, the unsubstituted amine derivative **48** was assayed, and it was also inactive. Inspired by the results, the analogues of compound **41** were tested for MDMX inhibitory activities. The results revealed that compounds **40**, **44**, **46**, and **47** showed moderate to good binding activity to MDMX, indicating that they were dual inhibitors of p53−MDM2/MDMX protein−protein interaction.

To further validate the mechanism of MDMX binding for compound **41**, Western immunoblotting was also used for analyzing the levels of p53, MDMX, and $p21^{cip1/waf}$ proteins in MCF-7 cancer cells (MDMX overexpression). Consistent with the result of the fluorescence polarization binding assay, compound **41** also caused a dose-dependent increase in the levels of p53, MDMX, and $p21^{cip1/waf}$ proteins after 24 h treatment in MCF-7 cells (Figure 6). The results also indicated a superior activation of p53 but no activity to phosphorylation-p53 (p-p53).

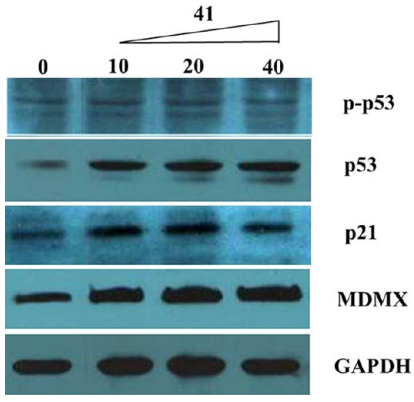

Figure 6. Cellular activity of **41** for the p53 pathway activation detected by Western blotting (MCF-7 cells, 24 h treatment).

Effect of Pyrrolidone Derivatives on Apoptosis in A549 Cells. The effect of compound **60a** and nutlin-3a on the induction of A549 cell apoptosis was evaluated by fluorescence-activated cell sorting (Figure 7). The results indicated that compound **60a** and nutlin-3a caused a dose-dependent increase in their apoptotic effect. When treated with 5 μM of **60a** and nutlin-3a, there were no obvious differences compared with the control group and DMSO group. After 48 h treatment, the percentage of apoptotic cells for compound **60a** and nutlin-3a was only 0.63% and 0.90%, respectively. At the concentration of 10 μM, the percentage of apoptotic cells for compound **60a** and nutlin-3a was increased to 4.02% and 6.46%, respectively. Visual assessment of the immunostaining suggested that some A549 cells became small, round, and floating. When the concentration was increased to 20 μM, a remarkable apoptotic effect was observed for compounds **60a** (17.85% apoptotic cells) and nutlin-3a (15.49% apoptotic cells).

In Vivo Antitumor Potency. To further test the therapeutic potential for the novel pyrrolidone p53−MDM2 inhibitors, compounds **41** and **60a** were chosen to evaluate their ability to inhibit tumor growth in the A549 xenograft model because of their potent p53−MDM2 inhibitory activity and antiproliferative activity. The results revealed that no toxicity or drug-related death was observed in the nude mice that were treated with the two compounds (200 mg/kg, orally, once daily) for 14 days. They were effective as oral agents, producing a tumor volume inhibition of about 40% (Figure 8A). Unlike irinotecan and doxorubicin, compounds **41** and **60a** had little effect on the body weight of the nude mice (Figure 8B).

Next, the ability of compound **60a** at 300 mg/kg to inhibit tumor growth in the A549 xenograft model was evaluated. After a 13-day incubation of A549 human cancer cells in the mice, compound **60a** was orally administered once daily for 14 days, and the tumor volume was monitored. The results revealed that compound **60a** is highly effective in inhibition of tumor growth as an oral agent. At 300 mg/kg, 52.53% tumor growth inhibition was achieved (Figure 9A). Moreover, there is no significant weight loss in animals treated with **60a** compared with those in the vehicle control group (Figure 9B).

CONCLUSION

A series of novel pyrrolidone inhibitors of p53−MDM2 protein−protein interaction were successfully identified by structure-based virtual screening. Further structural optimization and SAR studies led to the discovery of a number of nanomolar inhibitors. Results of biological evaluations highlighted the promising future of compounds **41** and **60a** as novel antitumor leads: (1) They represent a novel class of p53−MDM2 inhibitors with nanomolar inhibitory activity and druglike properties. (2) They showed in vitro antitumor potency better than that of nutlin-3a, with good selectivity against tumor cells with deleted p53. (3) They were orally active and able to effectively inhibit the tumor growth in the A549 xenograft model. (4) Compound **41** was proved to be a dual inhibitor of p53−MDM2/MDMX interaction. Further optimization studies are in progress.

EXPERIMENTAL SECTION

Chemistry. *General Methods.* All starting materials were commercially available and analytical pure. Melting points were measured on an uncorrected X-5 digital melting point apparatus (Gongyi City Yuhua Instrument Co., Ltd.; China). ^{1}H NMR and ^{13}C

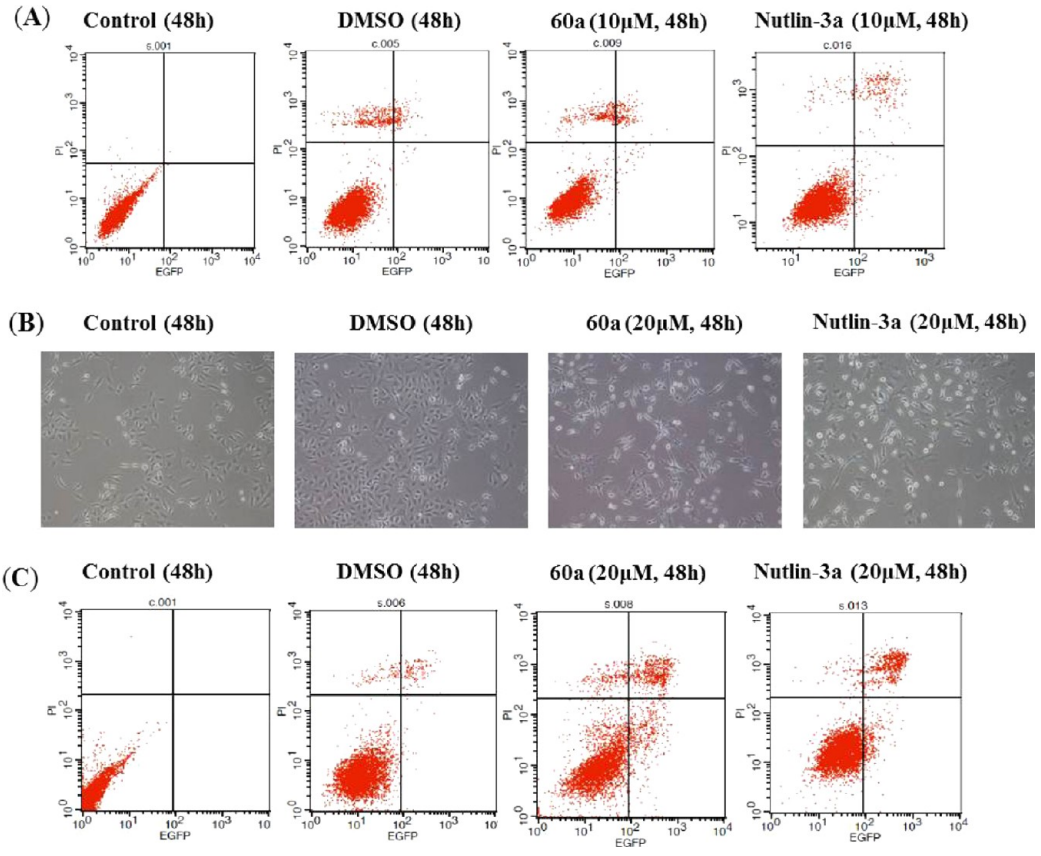

Figure 7. Pyrrolidone derivative-induced cell apoptosis. (A) A549 cells were treated with DMSO and 10 μM of compound **60a** for 48 h. (B) The effect of evodiamine derivatives on human cancer cell morphology. A549 cells were treated with DMSO and 20 μM of compound **60a** and nutlin-3a for 48 h, and representative photographs were captured under a light microscope. (C) A549 cells were treated with DMSO and 20 μM of compound **60a** for 48 h. Apoptosis was examined by flow cytometry (n = 3). Representative photographs from three independent experiments were displayed.

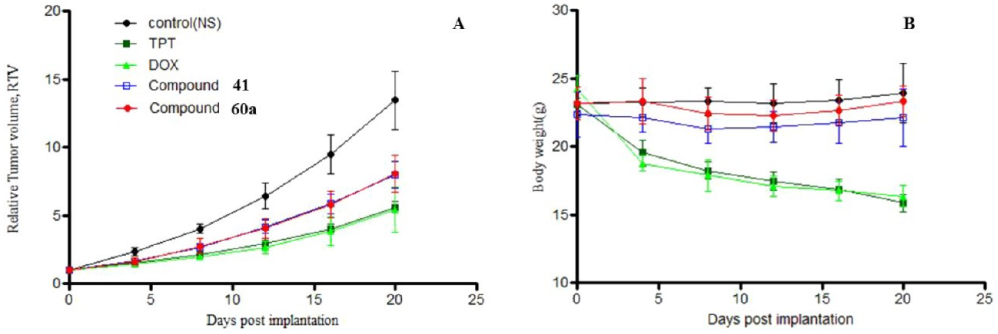

Figure 8. Inhibition of tumor growth for compounds **41** and **60a** (200 mg/kg, administered intragastrically) against A549 xenografts in nude mice: (A) relative tumor volume (RTV); (B) animal body weight.

NMR spectra were recorded on a Bruker AVANCE 300 spectrometer, a BRUKER AVANCE 500 spectrometer or a Bruker AVANCE 600 spectrometer (Bruker Company, Germany), using TMS as an internal standard and $CDCl_3$ or DMSO-d_6 as solvents. Chemical shifts (δ values) and coupling constants (J values) are given in ppm and hertz, respectively. Microwave reactions were performed on a Biotage microwave reactor. Elemental analyses were performed with a MOD-1106 instrument and were consistent with theoretical values within ±0.4%. TLC analysis was carried out on silica gel plates GF254 (Qindao Haiyang Chemical, China). Flash column chromatography was carried out on silica gel 300−400 mesh using a Biotage instrument. Anhydrous solvent and reagents were all analytical pure and dried through routine protocols.

*General Procedure A: Synthesis of Compound **11***. A solution of diethyl oxalate (12.0 mmol) and appropriate acetophenone (**10**, 6.0 mmol) in methanol (10 mL) was added dropwise to a fresh prepared solution of CH_3ONa in CH_3OH (2.6 mL of 25% w/v, 12.0 mmol), and the reaction was allowed to proceed under reflux for another 3 h. After cooling to room temperature, the reaction mixture was poured into water (40 mL) for 1 h, acidified with HCl (1 mL of 37% w/v) to reach pH 3−4, and extracted with diethyl ether (100 mL × 3). The combined organic extracts were washed with brine (30 mL), dried over Na_2SO_4, and filtered, and the solvent was removed in vacuum to afford the crude product **11** which was directly subjected to general procedure B.

*General Procedure B: Synthesis of Compounds **12**−**39***. Aldehyde (10 mmol) and *N*-(3-aminopropyl)imidazole (10 mmol) were mixed in 1, 4-dioxane (10 mL). After stirred for 15 min, a solution of compound **11** (10 mmol) in 1,4-dioxane (5 mL) was dropped slowly into the solvent. Then, the mixture was stirred for another 12 h. The

dx.doi.org/10.1021/jm300969t | J. Med. Chem. 2012, 55, 9630−9642

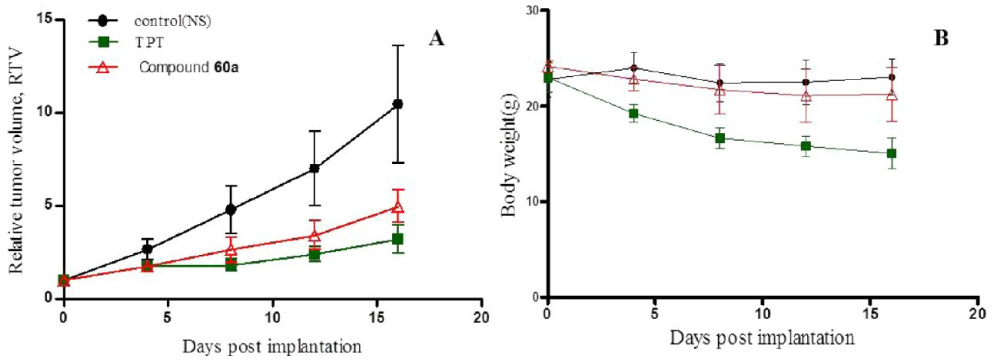

Figure 9. Inhibition of tumor growth for compound **60a** (300 mg/kg, administered intragastrically) against A549 xenografts in nude mice: (A) relative tumor volume (RTV); (B) animal body weight.

resulting precipitate was filtered off and recrystallized from CH_3OH to give compounds **12**–**39**.

*General Procedure C: Synthesis of Compounds **40**–**47**.* To a solution of compound **32** (1.0 mmol) in dry THF (20 mL) were added triphenylphosphine (1.5 mmol) and DIAD (1.5 mmol) at 0 °C under nitrogen atmosphere. The solution was stirred for 15 min at 0 °C, and then alcohol (10 mL) was added. The reaction mixture was stirred at room temperature overnight and concentrated under reduced pressure. The residue was purified by flash column chromatography (CH_2Cl_2:CH_3OH = 100: 1, v/v) to give compounds **40**–**47** (yields: 21.3–67.6%).

*General Procedure D: Synthesis of Compounds **49**–**60**.* A solution of compound **32** (1 mmol) and various amines (5 mmol) in acetic acid (5 mL) was subjected to microwave irradiation (120 °C, 2 h). After completion of reaction, the solution mixture was washed with water and then extracted by dichloromethane. The organic layer was washed with water and 2% aq $NaHCO_3$, separated, dried over Na_2SO_4, and evaporated to dryness. The residue was purified by flash column chromatography (CH_2Cl_2:CH_3OH = 100:1, v/v) to give compounds **49**–**60** (yields: 17.9–55.9%).

*1-(3-(1H-Imidazol-1-yl)propyl)-4-benzoyl-5-(4-bromophenyl)-3-ethoxy-1H-pyrrol-2(5H)-one (**40**).* Yield 33.9%, yellow solid, mp: 92–95 °C. ^{1}H NMR (600 MHz, DMSO-d_6) δ: 7.72 (m, 2H), 7.60 (m, 2H), 7.51 (m, 2H), 7.47 (m, 2H), 7.32 (m, 2H), 7.13 (s, 1H), 6.86 (s, 1H), 5.55 (s, 1H), 4.49 (m, 1H), 4.41 (m, 1H), 3.92 (m, 2H), 3.52 (m, 1H), 2.68 (m, 1H), 1.86 (m, 2H), 1.07 (t, 3H, J = 7.1 Hz). ^{13}C NMR (125 MHz, DMSO-d_6) δ: 190.17, 164.97, 151.06, 137.97, 137.70, 135.22, 133.62, 132.12, 130.53, 129.26, 128.75, 126.04, 122.14, 119.62, 67.63, 60.61, 43.96, 38.11, 29.41, 15.61. ESI-MS (m/z): 494.19 $[M + 1]^+$. Anal. ($C_{25}H_{24}BrN_3O_3$) C, H, N.

*1-(3-(1H-Imidazol-1-yl)propyl)-4-benzoyl-5-(4-bromophenyl)-3-isopropoxy-1H-pyrrol-2(5H)-one (**41**).* Yield 40.3%, white solid, mp: 122–123 °C. ^{1}H NMR (600 MHz, DMSO-d_6) δ: 7.67 (s, 1H), 7.66 (m, 1H), 7.59 (m, 2H), 7.52 (d, 2H, J = 8.5 Hz), 7.46 (t, 2H, J = 7.7 Hz), 7.31 (d, 2H, J = 8.5 Hz), 7.13 (s, 1H), 6.86 (s, 1H), 5.56 (s, 1H), 5.47 (m, 1H), 3.95 (m, 2H), 3.52 (m, 1H), 2.69 (m, 1H), 1.89 (m, 2H), 1.15 (d, 3H, J = 6.1 Hz), 1.01 (d, 3H, J = 6.1 Hz). ^{13}C NMR (150 MHz, DMSO-d_6) δ: 190.14, 165.03, 150.46, 137.97, 137.67, 135.33, 133.38, 132.16, 130.45, 129.21, 128.74, 128.60, 127.32, 122.10, 119.58, 74.14, 60.50, 43.97, 38.19, 29.40, 22.96, 22.86. ESI-MS (m/z): 508.15 $[M + 1]^+$. Anal. ($C_{26}H_{26}BrN_3O_3$) C, H, N.

*1-(3-(1H-Imidazol-1-yl)propyl)-4-benzoyl-5-(4-bromophenyl)-3-(pentyloxy)-1H-pyrrol-2(5H)-one (**42**).* Yield 34.7%, white solid, mp: 131–132 °C. ^{1}H NMR (600 MHz, DMSO-d_6) δ: 7.70 (m, 2H), 7.61 (t, 2H, J = 8.2 Hz), 7.52 (d, 2H, J = 7.2 Hz), 7.46 (t, 2H, J = 7.8 Hz), 7.34 (d, 2H, J = 8.5 Hz), 7.13 (s, 1H), 6.86 (s, 1H), 5.56 (s, 1H), 4.42 (m, 2H), 3.95 (m, 2H), 3.55 (m, 1H), 2.69 (m, 1H), 1.88 (m, 2H), 1.42 (m, 2H), 1.16 (m, 2H), 1.00 (m, 2H), 0.74 (t, 3H, J = 7.3 Hz). ^{13}C NMR (125 MHz, DMSO-d_6) δ: 190.15, 164.96, 151.29, 138.19, 137.64, 135.27, 133.41, 132.10, 130.49, 129.13, 128.68, 126.21, 122.10, 119.55, 71.51, 60.52, 43.95, 38.11, 29.40, 29.23, 27.43, 22.00, 14.12. ESI-MS (m/z): 536.29 $[M + 1]^+$. Anal. ($C_{28}H_{30}BrN_3O_3$) C, H, N.

*1-(3-(1H-Imidazol-1-yl)propyl)-4-benzoyl-5-(4-bromophenyl)-3-butoxy-1H-pyrrol-2(5H)-one (**43**).* Yield 67.6%, white solid, mp: 117–118 °C. ^{1}H NMR (600 MHz, DMSO-d_6) δ: 7.70 (m, 2H), 7.61 (m, 2H), 7.52 (d, 2H, J = 8.4 Hz), 7.46 (t, 2H, J = 7.8 Hz), 7.33 (d, 2H, J = 8.1 Hz), 7.13 (s, 1H), 6.86 (s, 1H), 5.55 (s, 1H), 4.38 (m, 2H), 3.96 (m, 2H), 3.53 (m, 1H), 2.69 (m, 1H), 1.89 (m, 2H), 1.41 (m, 2H), 1.07 (m, 2H), 0.73 (t, 3H, J = 7.4 Hz). ^{13}C NMR (125 MHz, DMSO-d_6) δ: 190.19, 164.97, 151.29, 138.18, 137.66, 135.27, 133.44, 132.12, 130.51, 129.14, 128.71, 126.16, 122.12, 119.57, 71.24, 60.56, 43.97, 38.14, 31.57, 29.40, 18.46, 13.79. ESI-MS (m/z): 522.26 $[M + 1]^+$. Anal. ($C_{27}H_{28}BrN_3O_3$) C, H, N.

*1-(3-(1H-Imidazol-1-yl)propyl)-4-benzoyl-5-(4-bromophenyl)-3-(cyclohexyloxy)-1H-pyrrol-2(5H)-one (**44**).* Yield 52.5%, light yellow solid, mp: 77–78 °C. ^{1}H NMR (600 MHz, DMSO-d_6) δ: 7.68 (m, 2H), 7.59 (m, 2H), 7.53 (d, 2H, J = 8.5 Hz), 7.46 (t, 2H, J = 7.7 Hz), 7.33 (d, 2H, J = 8.5 Hz), 7.12 (s, 1H), 6.86 (s, 1H), 5.58 (s, 1H), 5.52 (m, 1H), 3.93 (m, 2H), 3.53 (m, 1H), 2.69 (m, 1H), 1.88 (m, 2H), 1.78 (m, 2H), 1.60 (m, 2H), 1.31 (m, 6H). ^{13}C NMR (125 MHz, DMSO-d_6) δ: 190.10, 165.03, 150.50, 138.17, 137.66, 135.38, 133.34, 132.16, 130.45, 129.18, 128.77, 128.60, 127.72, 122.09, 119.57, 77.99, 60.47, 43.98, 38.18, 32.00, 29.41, 25.09, 22.47. ESI-MS (m/z): 548.17 $[M + 1]^+$. Anal. ($C_{29}H_{30}BrN_3O_3$) C, H, N.

*1-(3-(1H-Imidazol-1-yl)propyl)-4-benzoyl-3-(benzyloxy)-5-(4-bromophenyl)-1H-pyrrol-2(5H)-one (**45**).* Yield 40.1%, yellow solid, mp: 72–73 °C. ^{1}H NMR (600 MHz, DMSO-d_6) δ: 7.68 (m, 2H), 7.59 (m, 2H), 7.52 (d, 2H, J = 8.5 Hz), 7.42 (t, 2H, J = 7.8 Hz), 7.32 (d, 2H, J = 8.5 Hz), 7.27 (m, 3H), 7.13 (s, 1H), 7.10 (m, 2H), 6.87 (s, 1H), 5.59 (s, 1H), 5.53 (m, 2H), 3.95 (m, 2H), 3.57 (m, 1H), 2.72 (m, 1H), 1.89 (m, 2H). ^{13}C NMR (125 MHz, DMSO-d_6) δ: 189.96, 165.06, 150.70, 138.01, 137.68, 136.44, 135.10, 133.49, 132.14, 130.51, 129.21, 128.79, 128.76, 128.68, 128.55, 128.15, 127.45, 122.19, 119.56, 72.44, 60.60, 43.95, 38.13, 29.41. ESI-MS (m/z): 556.19 $[M + 1]^+$. Anal. ($C_{30}H_{26}BrN_3O_3$) C, H, N.

*1-(3-(1H-Imidazol-1-yl)propyl)-4-benzoyl-5-(4-bromophenyl)-3-(2-methoxyethoxy)-1H-pyrrol-2(5H)-one (**46**).* Yield 21.3%, white solid, mp: 62–63 °C. ^{1}H NMR (600 MHz, DMSO-d_6) δ: 7.70 (m, 2H), 7.61 (m, 2H), 7.53 (d, 2H, J = 8.5 Hz), 7.47 (t, 2H, J = 7.8 Hz), 7.32 (d, 2H, J = 8.5 Hz), 7.14 (s, 1H), 6.87 (s, 1H), 5.56 (s, 1H), 4.68 (m, 1H), 4.54 (m, 1H), 3.96 (m, 2H), 3.54 (m, 1H), 3.44 (m, 1H), 3.38 (m, 1H), 2.69 (m, 1H), 1.88 (m, 2H). ^{13}C NMR (125 MHz, DMSO-d_6) δ: 189.98, 164.94, 150.94, 137.94, 137.62, 135.25, 133.52, 132.12, 130.43, 129.24, 128.72, 128.54, 126.17, 122.12, 119.62, 71.20, 70.27, 60.52, 58.45, 43.98, 38.09, 29.37. ESI-MS (m/z): 524.20 $[M + 1]^+$. Anal. ($C_{26}H_{26}BrN_3O_4$) C, H, N.

*1-(3-(1H-Imidazol-1-yl)propyl)-4-benzoyl-5-(4-bromophenyl)-3-propoxy-1H-pyrrol-2(5H)-one (**47**).* Yield 64.1%, light yellow solid, mp: 101–103 °C. ^{1}H NMR (600 MHz, DMSO-d_6) δ: 7.71 (m, 2H), 7.61 (t, 2H, J = 7.7 Hz), 7.52 (d, 2H, J = 8.4 Hz), 7.47 (t, 2H, J = 7.8 Hz), 7.33 (d, 2H, J = 8.4 Hz), 7.13 (s, 1H), 6.86 (s, 1H), 5.56 (s, 1H), 4.39 (m, 2H), 3.96 (m, 2H), 3.54 (m, 1H), 2.70 (m, 1H), 1.90 (m, 2H), 1.45 (m, 2H), 0.64 (t, 3H, J = 7.4 Hz). ^{13}C NMR (125 MHz, DMSO-d_6) δ: 190.15, 164.96, 151.23, 138.14, 137.64, 135.26, 133.47, 132.10, 130.48, 129.15, 128.71, 128.66, 126.16, 122.11, 119.58, 73.04,

dx.doi.org/10.1021/jm300969t | J. Med. Chem. 2012, 55, 9630–9642

60.56, 43.98, 38.13, 29.39, 22.97, 10.16. ESI-MS (m/z): 508.42 $[M + 1]^+$. Anal. ($C_{26}H_{26}BrN_3O_3$) C, H, N.

*1-(3-(1H-Imidazol-1-yl)propyl)-3-amino-4-benzoyl-5-(4-bromophenyl)-1H-pyrrol-2(5H)-one (**48**).* To a solution of compound **32** (1 mmol) in 2-methoxyethanol (5 mL) was added ammonium formate (3 mmol) in a sealed tube. The solution was heated under microwave irradiation (150 °C, 1 h). The mixture was concentrated under vacuum, and the residue was triturated in ether. After filtration, the solid was washed with ether to give the crude compound, which was purified by flash column chromatography (CH_2Cl_2:CH_3OH = 100: 1, v/v) to give compound **48**, yield 32.0%, mp: 222−226 °C. ^{1}H NMR (500 MHz, DMSO-d_6) δ: 10.05 (s, 1H), 8.76 (s, 1H), 7.57 (s, 1H), 7.42 (m, 1H), 7.30−7.33 (m, 4H), 7.27 (d, 2H, J = 7.8 Hz), 7.10 (s, 1H), 6.85 (s, 1H), 6.63 (d, 2H, J = 7.9 Hz), 5.41 (s, 1H), 3.81−3.94 (m, 2H), 3.47 (m, 1H), 2.55 (m, 1H), 1.77−1.82 (m, 2H) . ^{13}C NMR (125 MHz, DMSO-d_6) δ: 179.97, 164.59, 163.61, 138.34, 137.64, 134.14, 131.30, 130.70, 129.86, 128.70, 127.99, 120.88, 119.59, 105.16, 58.47, 44.01, 38.31, 29.02. ESI-MS (m/z): 465.09 $[M + 1]^+$. Anal. ($C_{23}H_{21}BrN_4O_2$) C, H, N.

*1-(3-(1H-Imidazol-1-yl)propyl)-4-benzoyl-5-(4-bromophenyl)-3-(phenylamino)-1H-pyrrol-2(5H)-one (**49**).* Following general procedure D, compound **32** was reacted with phenylamine to afford compound **49** as dark yellow solid (Yield 52.1%), mp: 79−82 °C. ^{1}H NMR (500 MHz, DMSO-d_6) δ: 9.04 (s, 1H), 7.61 (s, 1H), 7.42 (d, 2H, J = 8.4 Hz), 7.34 (m, 3H), 7.11−7.17 (m, 5H), 6.77−6.98 (m, 6H), 5.63 (s, 1H), 3.96 (m, 2H), 3.58 (m, 1H), 2.74 (m, 1H), 1.90 (m, 2H). ^{13}C NMR (125 MHz, DMSO-d_6) δ: 190.63, 166.33, 140.86, 139.85, 139.50, 137.68, 136.73, 132.13, 131.87, 130.41, 128.73, 128.58, 128.37, 128.27, 123.22, 121.64, 121.24, 119.63, 116.68, 62.59, 44.06, 38.45, 29.44. ESI-MS (m/z): 541.57 $[M + 1]^+$. Anal. ($C_{29}H_{25}BrN_4O_2$) C, H, N.

*1-(3-(1H-Imidazol-1-yl)propyl)-4-benzoyl-5-(4-bromophenyl)-3-(p-tolylamino)-1H-pyrrol-2(5H)-one (**50**).* Yield 55.9%, dark yellow solid, mp: 90−92 °C. ^{1}H NMR (300 MHz, DMSO-d_6) δ: 9.04 (s, 1H), 7.59 (s, 1H), 7.30−7.39 (m, 6H), 7.06−7.20 (m, 5H), 6.78−6.85 (m, 4H), 5.61 (s, 1H), 3.94 (m, 2H), 3.54 (m, 1H), 2.49 (m, 1H), 2.11 (s, 3H), 1.82 (m, 2H). ^{13}C NMR (125 MHz, DMSO-d_6) δ: 190.56, 166.15, 140.63, 139.73, 138.08, 137.68, 136.83, 132.49, 131.94, 131.81, 130.38, 128.99, 128.78, 128.26, 128.19, 121.72, 121.56, 119.59, 115.81, 62.52, 44.02, 38.41, 29.43, 20.76. ESI-MS (m/z): 555.33 $[M + 1]^+$. Anal. ($C_{30}H_{27}BrN_4O_2$) C, H, N.

*1-(3-(1H-Imidazol-1-yl)propyl)-4-benzoyl-5-(4-bromophenyl)-3-((4-ethoxyphenyl)amino)-1H-pyrrol-2(5H)-one (**51**).* Yield 31.8%, dark yellow solid, mp: 179−182 °C. ^{1}H NMR (300 MHz, DMSO-d_6) δ: 9.04 (s, 1H), 7.59 (s, 1H), 7.39 (d, 2H, J = 8.4 Hz), 7.32 (m, 3H), 7.17 (m, 3H), 7.10 (d, 2H, J = 8.4 Hz), 6.83 (m, 3H), 6.56 (d, 2H, J = 9.0 Hz), 5.59 (s, 1H), 3.93 (m, 2H), 3.86 (q, 2H), 3.56 (m, 1H), 2.70 (m, 1H), 1.86 (m, 2H), 1.22 (m, 3H). ^{13}C NMR (125 MHz, DMSO-d_6) δ: 190.51, 166.06, 155.13, 141.35, 139.95, 137.67, 137.00, 133.53, 131.79, 130.38, 128.79, 128.25, 128.16, 123.64, 121.51, 119.60, 114.67, 114.57, 63.56, 62.43, 44.04, 38.39, 29.43, 15.07. ESI-MS (m/z): 585.40 $[M + 1]^+$. Anal. ($C_{31}H_{29}BrN_4O_3$) C, H, N.

*1-(3-(1H-Imidazol-1-yl)propyl)-4-benzoyl-5-(4-bromophenyl)-3-((4-fluorophenyl)amino)-1H-pyrrol-2(5H)-one (**52**).* Yield 41.9%, bright yellow solid, mp: 85−87 °C. ^{1}H NMR (600 MHz, DMSO-d_6) δ: 9.03 (s, 1H), 7.60 (s, 1H), 7.41 (d, 2H, J = 8.5 Hz), 7.34 (t, 3H, J = 9.1 Hz), 7.21 (d, 2H, J = 7.7 Hz), 7.15 (m, 3H), 6.99 (m, 3H), 6.81 (t, 2H, J = 8.7 Hz), 5.60 (s, 1H), 3.98 (m, 2H), 3.58 (m, 1H), 2.75 (m, 1H), 1.91 (m, 2H). ^{13}C NMR (125 MHz, DMSO-d_6) δ: 190.73, 166.39, 140.61, 139.74, 137.43, 136.84, 132.31, 131.99, 130.54, 128.86, 128.52, 128.40, 123.78, 123.72, 121.77, 121.38, 121.32, 119.79, 116.03, 62.72, 44.20, 38.59, 29.51. ESI-MS (m/z): 559.50 $[M + 1]^+$. Anal. ($C_{29}H_{24}BrFN_4O_2$) C, H, N.

*1-(3-(1H-Imidazol-1-yl)propyl)-4-benzoyl-5-(4-bromophenyl)-3-((4-iodophenyl)amino)-1H-pyrrol-2(5H)-one (**53**).* Yield 23.5%, dark yellow solid, mp: 85−87 °C. ^{1}H NMR (600 MHz, DMSO-d_6) δ: 9.10 (s, 1H), 7.72 (s, 1H), 7.34−7.41 (m, 12H), 6.93 (m, 1H), 6.71 (m, 2H), 5.63 (s, 1H), 3.96 (m, 2H), 3.57 (m, 1H), 2.73 (m, 1H), 1.91 (m, 2H). ^{13}C NMR (125 MHz, DMSO-d_6) δ: 190.80, 166.37, 140.95, 139.67, 139.51, 137.62, 137.25, 136.55, 132.47, 132.00, 130.54, 128.53, 128.41, 128.14, 123.65, 122.10, 121.82, 119.80, 116.03, 62.78, 44.40, 38.53, 29.41. ESI-MS (m/z): 667.40 $[M + 1]^+$. Anal. ($C_{29}H_{24}BrIN_4O_2$) C, H, N.

*1-(3-(1H-Imidazol-1-yl)propyl)-4-benzoyl-5-(4-bromophenyl)-3-((4-bromophenyl)amino)-1H-pyrrol-2(5H)-one (**54**).* Yield 43.5%, bright yellow solid, mp: 104−107 °C. ^{1}H NMR (300 MHz, DMSO-d_6) δ: 9.11 (s, 1H), 7.59 (s, 1H), 7.34−7.41 (m, 5H), 7.21 (d, 2H, J = 6.9 Hz), 7.13 (m, 5H), 7.10 (m, 3H), 5.61 (s, 1H), 3.93 (m, 2H), 3.56 (m, 1H), 2.71 (m, 1H), 1.85 (m, 2H). ^{13}C NMR (125 MHz, DMSO-d_6) δ: 190.48, 166.26, 140.45, 139.54, 139.43, 137.68, 136.53, 132.34, 131.88, 131.28, 130.44, 128.79, 128.41, 128.31, 123.21, 121.68, 119.60, 117.50, 114.87, 62.65, 44.02, 38.45, 29.42. ESI-MS (m/z): 619.15 $[M + 1]^+$. Anal. ($C_{29}H_{24}Br_2N_4O_2$) C, H, N.

*1-(3-(1H-Imidazol-1-yl)propyl)-4-benzoyl-5-(4-bromophenyl)-3-((4-chlorophenyl)amino)-1H-pyrrol-2(5H)-one (**55**).* Yield 43.6%, bright yellow solid, mp: 92−94 °C. ^{1}H NMR (600 MHz, DMSO-d_6) δ: 9.08 (s, 1H), 7.56 (s, 1H), 7.39 (d, 2H, J = 8.4 Hz), 7.34 (m, 3H), 7.10−7.30 (m, 5H), 7.00 (d, 2H, J = 9.0 Hz), 6.84 (m, 3H), 5.60 (s, 1H), 3.97 (m, 2H), 3.56 (m, 1H), 3.03 (m, 1H), 1.90 (m, 2H). ^{13}C NMR (125 MHz, DMSO-d_6) δ: 190.49, 166.27, 140.02, 139.65, 139.45, 137.69, 136.57, 132.32, 131.88, 130.44, 128.79, 128.40, 128.31, 126.87, 122.86, 121.68, 119.61, 117.32, 62.64, 44.02, 38.46, 29.42. ESI-MS (m/z): 575.75 $[M + 1]^+$. Anal. ($C_{29}H_{24}BrClN_4O_2$) C, H, N.

*1-(3-(1H-Imidazol-1-yl)propyl)-4-benzoyl-5-(4-bromophenyl)-3-((4-(trifluoromethoxy)phenyl)amino)-1H-pyrrol-2(5H)-one (**56**).* Yield 17.9%, bright yellow solid, mp: 70−71 °C. ^{1}H NMR (600 MHz, DMSO-d_6) δ: 9.05 (s, 1H), 7.58 (s, 1H), 7.41 (d, 2H, J = 8.4 Hz), 7.30 (m, 3H), 7.14 (m, 5H), 6.93 (m, 4H), 6.84 (s, 1H), 5.59 (s, 1H), 3.96 (m, 2H), 3.57 (m, 1H), 2.75 (m, 1H), 1.87 (m, 2H). ESI-MS (m/z): 625.82 $[M + 1]^+$. Anal. ($C_{30}H_{24}BrF_3N_4O_3$) C, H, N.

*1-(3-(1H-Imidazol-1-yl)propyl)-4-benzoyl-5-(4-bromophenyl)-3-((3-bromophenyl)amino)-1H-pyrrol-2(5H)-one (**57**).* Yield 42.0%, bright yellow solid, mp: 102−104 °C. ^{1}H NMR (300 MHz, DMSO-d_6) δ: 9.05 (s, 1H), 7.61 (s, 1H), 7.44 (d, 2H, J = 8.1 Hz), 7.35 (m, 3H), 7.18 (m, 5H), 6.91 (m, 5H), 5.63 (s, 1H), 3.96 (m, 2H), 3.58 (m, 1H), 2.74 (m, 1H), 1.86 (m, 2H). ^{13}C NMR (125 MHz, DMSO-d_6) δ: 190.61, 166.42, 142.98, 139.21, 138.86, 137.69, 136.48, 132.41, 131.93, 130.45, 128.75, 128.46, 128.22, 125.46, 123.37, 121.75, 121.60, 119.89, 119.63, 118.04, 62.63, 44.02, 38.43, 29.44. ESI-MS (m/z): 619.70 $[M - 1]^-$. Anal. ($C_{29}H_{24}Br_2N_4O_2$) C, H, N.

*1-(3-(1H-Imidazol-1-yl)propyl)-4-benzoyl-5-(4-bromophenyl)-3-((2-bromophenyl)amino)-1H-pyrrol-2(5H)-one (**58**).* Yield 47.1%, bright yellow solid, mp: 89−91 °C. ^{1}H NMR (600 MHz, DMSO-d_6) δ: 8.81 (s, 1H), 7.63 (s, 1H), 7.35−7.40 (m, 5H), 7.21 (m, 2H), 7.10−7.18 (m, 5H), 6.88 (m, 2H), 5.69 (s, 1H), 3.95 (m, 2H), 3.55 (m, 1H), 2.71 (m, 1H), 1.89 (m, 2H). ^{13}C NMR (125 MHz, DMSO-d_6) δ: 190.88, 165.33, 141.12, 139.36, 138.47, 137.65, 136.26, 132.77, 132.10, 131.89, 130.48, 128.56, 128.49, 128.05, 127.99, 126.30, 125.11, 121.72, 119.70, 117.82, 117.40, 62.34, 44.09, 38.39, 29.41. ESI-MS (m/z): 619.15 $[M + 1]^+$. Anal. ($C_{29}H_{24}Br_2N_4O_2$) C, H, N.

*1-(3-(1H-Imidazol-1-yl)propyl)-4-benzoyl-3-(benzylamino)-5-(4-bromophenyl)-1H-pyrrol-2(5H)-one (**59**).* Yield 36.0%, light yellow solid, mp: 66−68 °C. ^{1}H NMR (500 MHz, DMSO-d_6) δ: 7.58 (s, 1H), 7.34−7.39 (m, 8H), 7.24−7.29 (m, 5H), 7.11 (s, 1H), 6.87 (s, 1H), 6.76 (d, 2H, J = 8.4 Hz), 5.61 (s, 1H), 5.03 (s, 1H), 3.94 (m, 2H), 3.48 (m, 2H), 3.39 (m, 1H), 2.60 (m, 1H), 1.85 (m, 2H). ESI-MS (m/z): 555.48 $[M + 1]^+$. Anal. ($C_{30}H_{27}BrN_4O_2$) C, H, N.

*(R)-1-(3-(1H-Imidazol-1-yl)propyl)-4-benzoyl-5-(4-bromophenyl)-3-(((R)-1-phenylethyl)amino)-1H-pyrrol-2(5H)-one (**60a**).* Yield 6.93%, light yellow solid, mp: 92−93 °C. ^{1}H NMR (300 MHz, DMSO-d_6) δ: 7.53 (s, 1H), 7.34−7.39 (m, 7H), 7.24−7.29 (m, 5H), 7.06 (s, 1H), 6.83 (s, 1H), 6.77 (d, 2H, J = 8.1 Hz), 6.01 (bar, 1H), 5.63 (s, 1H), 3.90 (m, 2H), 3.47 (m, 1H), 2.57 (m, 1H), 1.82 (m, 1H), 1.79 (m, 2H), 1.59 (d, 3H, J = 6.9 Hz). ^{13}C NMR (75 MHz, DMSO-d_6) δ: 192.17, 165.69, 146.18, 141.87, 139.05, 138.27, 132.94, 132.27, 131.60, 130.50, 130.18, 130.04, 129.80, 129.03, 128.72, 127.84, 122.68, 120.98, 113.46, 62.63, 52.22, 45.33, 39.42, 30.62, 25.45. ESI-MS (m/z): 569.15 $[M + 1]^+$. Anal. ($C_{31}H_{29}BrN_4O_2$) C, H, N. $[\alpha]_D$ = −298.9° (c = 0.540 in CH_3OH).

*(R)-1-(3-(1H-Imidazol-1-yl)propyl)-4-benzoyl-5-(4-bromophenyl)-3-(((S)-1-phenylethyl)amino)-1H-pyrrol-2(5H)-one (**60b**).* Yield

dx.doi.org/10.1021/jm300969t | J. Med. Chem. 2012, 55, 9630−9642

10.3%, light yellow solid, mp: 75−76 °C. ^{1}H NMR (300 MHz, DMSO-d_6) δ: 7.99 (s, 1H), 7.21−7.33 (m, 13H), 7.00 (s, 1H), 6.72 (m, 2H), 6.77 (d, 2H, J = 8.1 Hz), 5.87 (bar, 1H), 5.64 (s, 1H), 3.99 (m, 2H), 3.39 (m, 1H), 2.50 (m, 1H), 2.07 (m, 1H), 1.85 (m, 2H), 1.53 (d, 3H, J = 6.9 Hz). ^{13}C NMR (75 MHz, DMSO-d_6) δ: 192.22, 166.01, 145.84, 141.82, 139.83, 133.00, 132.52, 131.55, 130.47, 130.15, 129.99, 129.85, 129.01, 128.91, 127.77, 122.79, 122.19, 120.92, 113.86, 62.92, 52.79, 46.12, 39.23, 30.47, 25.78. ESI-MS (m/z): 569.15 [M + 1]$^+$. Anal. ($C_{31}H_{29}BrN_4O_2$) C, H, N. $[\alpha]_D$ = −45.93° (c = 0.540 in CH_3OH).

Fluorescence Polarization Binding Assay. All fluorescence experiments were performed as described in the literature.[22,23,36] Briefly, the fluorescence polarization experiments were read on Biotek Synergy H4 with the 485 nm excitation and 535 nm emission filters. The fluorescence intensities parallel (Intparallel) and perpendicular (Intperpedicular) to the plane of excitation were measured in black 96-well NBS assay plates (Corning #3993) at room temperature. The background fluorescence intensities of blank samples containing the reference buffer were subtracted, and steady-state fluorescence polarization was calculated using the following equation: P = 1000 × (Intparallel − GIntperpedicular)/(Intparallel + GIntperpedicular), and the correction factor G (G = 0.998 determined empirically) was introduced to eliminate differences in the transmission of vertically and horizontally polarized light. All fluorescence polarization values were expressed in millipolarization units (mP). The dose-dependent binding experiments were carried out with serial dilution in DMSO of compounds. A 5 μL sample of the test sample, preincubated (for 30 min) MDM2 binding domain (1−118) (10 nM) or MDMX binding domain (1−137) (120 nM), and PMDM-F peptide (Anaspec) (10 nM) in assay buffer (100 mM potassium phosphate, pH 7.5; 100 mg/mL bovine gamma globulin; 0.02% sodium azide) were added to microplates to produce a final volume of 115 μL. For each assay, the controls contained the MDM2/X binding domain and PMDM-F. Plates were read at 1 h after mixing all assay components. Binding constant (K_i) and inhibition curves were fitted using GraphPad Prism software. Nutlin-3a (Sigma-Aldrich) was used as reference compound for validating the assay in each plate. Details of protein expression and purification can be found in Supporting Information.

In Vitro Antiproliferative Assay. The cellular growth inhibitory activity was determined using two human osteosarcoma cell lines [U-2 OS (wild type p53) and Saos-2 (p53 null)] and two human lung cancer cell lines [A549 (wild-type p53) and NCI-H1299 (p53 null)]. An amount of 5−6 × 10^4 cells per well was transferred to 96-well plates. After culturing for 24 h, the test compounds were added to triplicate wells at different concentrations and 0.1% DMSO for control. After 72 h of incubation, 20 μL of MTT (3-[4,5-dimethylthiazol-2-yl]-2,5-diphenyltetrazolium bromide) solution (5 mg/mL) was added to each well, and after the samples were shaken for 1 min, the plate was incubated further for 4 h at 37 °C. Pyrrolidones were dissolved in 100 μL of DMSO. The absorbance (OD) was quantitated with the microplates using Biotek Synergy H4 at 570 nm. Wells containing no drugs were used as blanks. The concentration of the compounds that inhibited cell growth by 50% (IC_{50}) was calculated.

Western Blot Assay. A549 and MCF-7 cancer cell lines with wild-type p53 were grown in the recommended media supplemented with 10% FBS (Invitrogen) in a humidified environment with 5% CO_2. After 48 h treatment with various concentrations of compounds, cells were lysed and the protein extract was denatured and run on 5% Tris-glycine polyacrylamide gels (Invitrogen). Gels were electroblotted onto nitrocellulose membranes, and Western detection was carried out using 5% milk buffer (5% nonfat dry milk in TBS/0.1% tween-20) throughout. Proteins were detected by ECL chemiluminescence reagents (Amersham, Piscataway, NJ) using antibodies specific for human p53 (Calbiochem, cat. no. OP43T), p-p53 (Ser-15) (Cell Signaling, cat. no. 9286S), p21 (BD Biosciences, cat. no. 556430), MDM2 (Millipore, cat. no. 07−575), MDMX (abcam, cat. no. ab16058), and GAPDH(2A8)Mouse mAb (abmart, cat. no. M20028S).

Cell Apoptosis Assay. A549 cells (5 × 10^5 cells/mL) were seeded in six-well plates and treated with compounds at concentrations of 5−20 μM for 48 h. The cells were then harvested by trypsinization and washed twice with cold PBS. After centrifugation and removal of the supernatants, cells were resuspended in 400 μL of 1 × binding buffer which was then added to 5 μL of annexin V-FITC and incubated at room temperature for 15 min. After addition of 10 μL of PI, the cells were incubated at room temperature for another 15 min in the dark. The stained cells were analyzed by a flow cytometer (BD Accuri C6).

In Vivo Antiproliferative Assay. The in vivo antitumor activity of compounds **41** and **60a** was evaluated. Irinotecan (IRT) and doxorubicin (DOX) were used as reference drugs. BALB/C nude male mice (Certificate SCXK2003-0003, weighing 18−20 g) were obtained from Shanghai Experimental Animal Center, Chinese Academy of Sciences. A549 cancer cell suspensions were implanted subcutaneously into the right axilla region of the mice. Treatment began when implanted tumors had reached a volume of 100−300 mm^3 (after 13 days). The animals were randomized into appropriate groups (6 animals per treatment and 10 animals for the control group) and administered by gavage once daily for 14 consecutive days from day 13 after implantation of the cells. Tumor volumes were monitored by caliper measurement of the length and width and then calculated using the formula of TV = 1/2 × a × b^2, where a is the tumor length and b is the width. Tumor volumes and bodyweights were monitored every 4 days over the course of treatment. Mice were sacrificed on day 29 or 33 after implantation of cells, and tumors were removed and recorded for analysis. Irinotecan (0.5 mg/kg, Jiangsu Aosaikang Pharmacetical, China) was administered intravenously once daily for 5 consecutive days. Doxorubicin (10 mg/kg, Pfizer Italia S.r.l) was administered intravenously once.

Computational Protocols. Molecular docking was used to predict the binding mode of the p53−MDM2 inhibitors. The crystal structure of MDM2 (PDB code: 1T4E)[20] was prepared by removing the ligand and adding hydrogen atoms in Discovery Studio 2.5[49] software package. GOLD[23,50,51] with the GoldScore fitness function was used for molecular docking with default parameters. The reliability of the docking poses was further validated by MD simulations. Desmond[52−54] was used to carry out the entire simulation, while the systems were modeled with the OPLS-AA force field. The docked conformations of compounds (**1**, **5**, **6**, **9**) and MDM2 complexes were respectively neutralized by adding salt counterion, and the concentration was set to 0.15 using a system builder package. As a result, complexes were immersed in a cubic box (15 Å) containing about 11 689 TIP3P water molecules, respectively. Other parameters were default values. The systems were then simulated for 2 ns at 300 K and 1 atm. System coordinates were saved every 4.8 ps for further analysis, and heavy atom RMSD from the energy-minimized model structure was calculated for each MD snapshot. After 2 ns of MD calculations, stable MDM2−inhibitor complexes were obtained. The MD results indicated that the binding poses of the hits were very similar to those obtained from the molecular docking model (RMSD < 2 Å).

■ ASSOCIATED CONTENT

Supporting Information

Computational details for virtual screening, structural characterization for compounds **12**−**39**, ECD calculations, binding mode for the two diastereoisomers of compound **60**, experimental details for protein expression and purification, reversibly binding assay, aqueous solubility of the selected inhibitors, and analysis of the selectivity of the pyrrolidone p53−MDM2 inhibitors over A2-S100A10 protein−protein interaction. This material is available free of charge via the Internet at http://pubs.acs.org.

■ AUTHOR INFORMATION

Corresponding Author

*(W.N.Z.) Phone/fax: 86-21-81871243; e-mail: zhangwnk@hotmail.com. (C.Q.S.) Phone/fax: 86-21-81871239; e-mail: shengcq@hotmail.com.

Author Contributions

[†]These two authors contributed equally to this work.

Notes

The authors declare no competing financial interest.

■ ACKNOWLEDGMENTS

This work was supported by the National Natural Science Foundation of China (grant 81222044, 30930107), the 863 Hi-Tech Program of China (grant 2012AA020302), Key Project of Science and Technology of Shanghai (no. 09431901700), Shanghai Rising-Star Program (grant 12QH1402600), and Shanghai Municipal Health Bureau (grant XYQ2011038). We thank Dr. Chuanxu Liu from School of Medicine, Shanghai Jiao Tong University, for technical assistance on the p53−MDM2/X binding assay.

■ ABBREVIATIONS USED

MDM2, murine double minute 2; FP, fluorescence polarization; MD, molecular dynamics; SAR, structure−activity relationship; ECD, electronic circular dichroism; DIAD, diisopropyl azodicarboxylate; IC_{50}, 50% inhibitory concentration; IRT, irinotecan; DOX, doxorubicin; p-p53, phosphorylation-p53; FBS, fetal bovine serum; RMSD, root-mean-square deviation; NBS, nonbinding surface; RTV, relative tumor volume

■ REFERENCES

(1) Levine, A. J. p53, the cellular gatekeeper for growth and division. *Cell* **1997**, *88*, 323−331.
(2) Vogelstein, B.; Lane, D.; Levine, A. J. Surfing the p53 network. *Nature* **2000**, *408*, 307−310.
(3) Chene, P. Inhibiting the p53−MDM2 interaction: an important target for cancer therapy. *Nat. Rev. Cancer* **2003**, *3*, 102−109.
(4) Hainaut, P.; Hollstein, M. p53 and human cancer: the first ten thousand mutations. *Adv. Cancer Res.* **2000**, *77*, 81−137.
(5) Cochran, A. G. Antagonists of protein-protein interactions. *Chem. Biol.* **2000**, *7*, R85−94.
(6) Oliner, J. D.; Kinzler, K. W.; Meltzer, P. S.; George, D. L.; Vogelstein, B. Amplification of a gene encoding a p53-associated protein in human sarcomas. *Nature* **1992**, *358*, 80−83.
(7) Oliner, J. D.; Pietenpol, J. A.; Thiagalingam, S.; Gyuris, J.; Kinzler, K. W.; Vogelstein, B. Oncoprotein MDM2 conceals the activation domain of tumour suppressor p53. *Nature* **1993**, *362*, 857−860.
(8) Picksley, S. M.; Lane, D. P. The p53-mdm2 autoregulatory feedback loop: a paradigm for the regulation of growth control by p53? *Bioessays* **1993**, *15*, 689−690.
(9) Wu, X.; Bayle, J. H.; Olson, D.; Levine, A. J. The p53-mdm-2 autoregulatory feedback loop. *Genes Dev.* **1993**, *7*, 1126−1132.
(10) Cochran, A. G. Protein-protein interfaces: mimics and inhibitors. *Curr. Opin. Chem. Biol.* **2001**, *5*, 654−659.
(11) Fry, D. C. Protein-protein interactions as targets for small molecule drug discovery. *Biopolymers* **2006**, *84*, 535−552.
(12) Kussie, P. H.; Gorina, S.; Marechal, V.; Elenbaas, B.; Moreau, J.; Levine, A. J.; Pavletich, N. P. Structure of the MDM2 oncoprotein bound to the p53 tumor suppressor transactivation domain. *Science* **1996**, *274*, 948−953.
(13) Millard, M.; Pathania, D.; Grande, F.; Xu, S.; Neamati, N. Small-molecule inhibitors of p53−MDM2 interaction: the 2006−2010 update. *Curr. Pharm. Des.* **2011**, *17*, 536−559.
(14) Kumar, S. K.; Hager, E.; Pettit, C.; Gurulingappa, H.; Davidson, N. E.; Khan, S. R. Design, synthesis, and evaluation of novel boronic-chalcone derivatives as antitumor agents. *J. Med. Chem.* **2003**, *46*, 2813−2815.
(15) Stoll, R.; Renner, C.; Hansen, S.; Palme, S.; Klein, C.; Belling, A.; Zeslawski, W.; Kamionka, M.; Rehm, T.; Muhlhahn, P.; Schumacher, R.; Hesse, F.; Kaluza, B.; Voelter, W.; Engh, R. A.; Holak, T. A. Chalcone derivatives antagonize interactions between the human oncoprotein MDM2 and p53. *Biochemistry* **2001**, *40*, 336−344.
(16) Luke, R. W. A.; Jewsbury, P. J.; Cotton, R. Piperazine-4-phenyl derivatives as inhibitors of the interaction between mdm2 and p53. EP1112284, 2001.
(17) Duncan, S. J.; Gruschow, S.; Williams, D. H.; McNicholas, C.; Purewal, R.; Hajek, M.; Gerlitz, M.; Martin, S.; Wrigley, S. K.; Moore, M. Isolation and structure elucidation of Chlorofusin, a novel p53−MDM2 antagonist from a Fusarium sp. *J. Am. Chem. Soc.* **2001**, *123*, 554−560.
(18) Vassilev, L. T.; Vu, B. T.; Graves, B.; Carvajal, D.; Podlaski, F.; Filipovic, Z.; Kong, N.; Kammlott, U.; Lukacs, C.; Klein, C.; Fotouhi, N.; Liu, E. A. In vivo activation of the p53 pathway by small-molecule antagonists of MDM2. *Science* **2004**, *303*, 844−848.
(19) Galatin, P. S.; Abraham, D. J. A nonpeptidic sulfonamide inhibits the p53−mdm2 interaction and activates p53-dependent transcription in mdm2-overexpressing cells. *J. Med. Chem.* **2004**, *47*, 4163−4165.
(20) Grasberger, B. L.; Lu, T.; Schubert, C.; Parks, D. J.; Carver, T. E.; Koblish, H. K.; Cummings, M. D.; LaFrance, L. V.; Milkiewicz, K. L.; Calvo, R. R.; Maguire, D.; Lattanze, J.; Franks, C. F.; Zhao, S.; Ramachandren, K.; Bylebyl, G. R.; Zhang, M.; Manthey, C. L.; Petrella, E. C.; Pantoliano, M. W.; Deckman, I. C.; Spurlino, J. C.; Maroney, A. C.; Tomczuk, B. E.; Molloy, C. J.; Bone, R. F. Discovery and cocrystal structure of benzodiazepinedione HDM2 antagonists that activate p53 in cells. *J. Med. Chem.* **2005**, *48*, 909−912.
(21) Yin, H.; Lee, G. I.; Park, H. S.; Payne, G. A.; Rodriguez, J. M.; Sebti, S. M.; Hamilton, A. D. Terphenyl-based helical mimetics that disrupt the p53/HDM2 interaction. *Angew. Chem., Int. Ed.* **2005**, *44*, 2704−2707.
(22) Ding, K.; Lu, Y.; Nikolovska-Coleska, Z.; Qiu, S.; Ding, Y.; Gao, W.; Stuckey, J.; Krajewski, K.; Roller, P. P.; Tomita, Y.; Parrish, D. A.; Deschamps, J. R.; Wang, S. Structure-based design of potent nonpeptide MDM2 inhibitors. *J. Am. Chem. Soc.* **2005**, *127*, 10130−10131.
(23) Lu, Y.; Nikolovska-Coleska, Z.; Fang, X.; Gao, W.; Shangary, S.; Qiu, S.; Qin, D.; Wang, S. Discovery of a nanomolar inhibitor of the human murine double minute 2 (MDM2)−p53 interaction through an integrated, virtual database screening strategy. *J. Med. Chem.* **2006**, *49*, 3759−3762.
(24) Mohammad, R. M.; Wu, J.; Azmi, A. S.; Aboukameel, A.; Sosin, A.; Wu, S.; Yang, D.; Wang, S.; Al-Katib, A. M. An MDM2 antagonist (MI-319) restores p53 functions and increases the life span of orally treated follicular lymphoma bearing animals. *Mol. Cancer* **2009**, *8*, 115.
(25) Azmi, A. S.; Aboukameel, A.; Banerjee, S.; Wang, Z.; Mohammad, M.; Wu, J.; Wang, S.; Yang, D.; Philip, P. A.; Sarkar, F. H.; Mohammad, R. M. MDM2 inhibitor MI-319 in combination with cisplatin is an effective treatment for pancreatic cancer independent of p53 function. *Eur. J. Cancer* **2010**, *46*, 1122−1131.
(26) Bernard, D.; Zhao, Y.; Wang, S. AM-8553: A Novel MDM2 Inhibitor with a Promising Outlook for Potential Clinical Development. *J. Med. Chem.* **2012**, *55*, 4934−4935.
(27) Rew, Y.; Sun, D.; Gonzalez-Lopez De Turiso, F.; Bartberger, M. D.; Beck, H. P.; Canon, J.; Chen, A.; Chow, D.; Deignan, J.; Fox, B. M.; Gustin, D.; Huang, X.; Jiang, M.; Jiao, X.; Jin, L.; Kayser, F.; Kopecky, D. J.; Li, Y.; Lo, M. C.; Long, A. M.; Michelsen, K.; Oliner, J. D.; Osgood, T.; Ragains, M.; Saiki, A. Y.; Schneider, S.; Toteva, M.; Yakowec, P.; Yan, X.; Ye, Q.; Yu, D.; Zhao, X.; Zhou, J.; Medina, J. C.; Olson, S. H. Structure-Based Design of Novel Inhibitors of the MDM2−p53 Interaction. *J. Med. Chem.* **2012**, *55*, 4936−4954.
(28) Hu, C. Q.; Hu, Y. Z. Small molecule inhibitors of the p53−MDM2. *Curr. Med. Chem.* **2008**, *15*, 1720−1730.
(29) Information from www.clinicaltrials.gov. (a) RG7112 (Hoffmann-La Roche). (b) RO5503781 (Hoffmann-La Roche). (c) MK-8242 (Merck).
(30) Zhuang, C.; Miao, Z.; Zhu, L.; Zhang, Y.; Guo, Z.; Yao, J.; Dong, G.; Wang, S.; Liu, Y.; Chen, H.; Sheng, C.; Zhang, W. Synthesis and biological evaluation of thio-benzodiazepines as novel small molecule

inhibitors of the p53−MDM2 protein-protein interaction. *Eur. J. Med. Chem.* **2011**, *46*, 5654−5661.
(31) Drysdale, M. J.; Hind, S. L.; Jansen, M.; Reinhard, J. F., Jr. Synthesis and SAR of 4-aryl-2-hydroxy-4-oxobut-2-enoic acids and esters and 2-amino-4-aryl-4-oxobut-2-enoic acids and esters: potent inhibitors of kynurenine-3-hydroxylase as potential neuroprotective agents. *J. Med. Chem.* **2000**, *43*, 123−127.
(32) Sechi, M.; Bacchi, A.; Carcelli, M.; Compari, C.; Duce, E.; Fisicaro, E.; Rogolino, D.; Gates, P.; Derudas, M.; Al-Mawsawi, L. Q.; Neamati, N. From ligand to complexes: inhibition of human immunodeficiency virus type 1 integrase by *β*-diketo acid metal complexes. *J. Med. Chem.* **2006**, *49*, 4248−4260.
(33) Gein, V. L.; Kasimova, N. N. Three-component synthesis of 4-acyl-1-(2-aminoethyl)-5-aryl-3-hydroxy-2,5-dihydropyrrol-2(1*H*)-ones. *Russian J. Gen. Chem.* **2002**, *72*, 1150−1151.
(34) Shoichet, B. K. Virtual screening of chemical libraries. *Nature* **2004**, *432*, 862−865.
(35) http://www.specs.net/.
(36) Popowicz, G. M.; Czarna, A.; Wolf, S.; Wang, K.; Wang, W.; Domling, A.; Holak, T. A. Structures of low molecular weight inhibitors bound to MDMX and MDM2 reveal new approaches for p53-MDMX/MDM2 antagonist drug discovery. *Cell Cycle* **2010**, *9*, 1104−1111.
(37) Reddy, T. R.; Li, C.; Guo, X.; Myrvang, H. K.; Fischer, P. M.; Dekker, L. V. Design, synthesis, and structure−activity relationship exploration of 1-substituted 4-aroyl-3-hydroxy-5-phenyl-1*H*-pyrrol-2(5*H*)-one analogues as inhibitors of the annexin A2-S100A10 protein interaction. *J. Med. Chem.* **2011**, *54*, 2080−2094.
(38) Gomez-Monterrey, I.; Bertamino, A.; Porta, A.; Carotenuto, A.; Musella, S.; Aquino, C.; Granata, I.; Sala, M.; Brancaccio, D.; Picone, D.; Ercole, C.; Stiuso, P.; Campiglia, P.; Grieco, P.; Ianelli, P.; Maresca, B.; Novellino, E. Identification of the Spiro(oxindole-3,3′-thiazolidine)-Based Derivatives as Potential p53 Activity Modulators. *J. Med. Chem.* **2010**, *53*, 8319−8329.
(39) Hardcastle, I. R.; Liu, J.; Valeur, E.; Watson, A.; Ahmed, S. U.; Blackburn, T. J.; Bennaceur, K.; Clegg, W.; Drummond, C.; Endicott, J. A.; Golding, B. T.; Griffin, R. J.; Gruber, J.; Haggerty, K.; Harrington, R. W.; Hutton, C.; Kemp, S.; Lu, X.; McDonnell, J. M.; Newell, D. R.; Noble, M. E.; Payne, S. L.; Revill, C. H.; Riedinger, C.; Xu, Q.; Lunec, J. Isoindolinone inhibitors of the murine double minute 2 (MDM2)−p53 protein−protein interaction: structure−activity studies leading to improved potency. *J. Med. Chem.* **2011**, *54*, 1233−1243.
(40) Liu, M.; Li, C.; Pazgier, M.; Mao, Y.; Lv, Y.; Gu, B.; Wei, G.; Yuan, W.; Zhan, C.; Lu, W. Y.; Lu, W. D-peptide inhibitors of the p53−MDM2 interaction for targeted molecular therapy of malignant neoplasms. *Proc. Natl. Acad. Sci. U.S.A.* **2010**, *107*, 14321−14326.
(41) Marine, J. C. MDM2 and MDMX in cancer and development. *Curr. Top. Dev. Biol.* **2011**, *94*, 45−75.
(42) Bassett, E. A.; Wang, W.; Rastinejad, F.; El-Deiry, W. S. Structural and functional basis for therapeutic modulation of p53 signaling. *Clin. Cancer Res.* **2008**, *14*, 6376−6386.
(43) Marine, J. C.; Dyer, M. A.; Jochemsen, A. G. MDMX: from bench to bedside. *J. Cell Sci.* **2007**, *120*, 371−378.
(44) Toledo, F.; Wahl, G. M. Regulating the p53 pathway: in vitro hypotheses, in vivo veritas. *Nat. Rev. Cancer* **2006**, *6*, 909−923.
(45) Wade, M.; Wahl, G. M. Targeting Mdm2 and Mdmx in cancer therapy: better living through medicinal chemistry? *Mol Cancer Res* **2009**, *7*, 1−11.
(46) Cheok, C. F.; Lane, D. P. New Developments in Small Molecules Targeting p53 Pathways in Anticancer Therapy. *Drug Dev. Res.* **2008**, *69*, 289−296.
(47) Doemling, A. Selective and dual-action p53/mdm2/mdm4 antagonists. WO 2008130614, 2008.
(48) Wade, M.; Wong, E. T.; Tang, M.; Stommel, J. M.; Wahl, G. M. Hdmx modulates the outcome of p53 activation in human tumor cells. *J. Biol. Chem.* **2006**, *281*, 33036−33044.
(49) Accelrys Software Inc., S. D. http://www.accelrys.com.
(50) Jones, G.; Willett, P.; Glen, R. C.; Leach, A. R.; Taylor, R. Development and validation of a genetic algorithm for flexible docking. *J. Mol. Biol.* **1997**, *267*, 727−748.
(51) Verdonk, M. L.; Cole, J. C.; Hartshorn, M. J.; Murray, C. W.; Taylor, R. D. Improved protein-ligand docking using GOLD. *Proteins* **2003**, *52*, 609−623.
(52) Bowers, K. J.; Dror, R. O.; Shaw, D. E. The midpoint method for parallelization of particle simulations. *J. Chem. Phys.* **2006**, *124*, 184109.
(53) Shaw, D. E. A fast, scalable method for the parallel evaluation of distance-limited pairwise particle interactions. *J. Comput. Chem.* **2005**, *26*, 1318−1328.
(54) Desmond_Maestro_academic-2009−02, V. http://www.deshawresearch.com.